Properties of Slow, Cumulative Sodium Channel Inactivation in Rat Hippocampal CA1 Pyramidal Neurons

Timothy Mickus, Hae-yoon Jung, and Nelson Spruston
Department of Neurobiology and Physiology, Institute for Neuroscience, Northwestern University, Evanston, Illinois 60208-3520 USA

ABSTRACT Sodium channels in the somata and dendrites of hippocampal CA1 pyramidal neurons undergo a form of long-lasting, cumulative inactivation that is involved in regulating back-propagating action potential amplitude and can influence dendritic excitation. Using cell-attached patch-pipette recordings in the somata and apical dendrites of CA1 pyramidal neurons, we determined the properties of slow inactivation on response to trains of brief depolarizations. We find that the amount of slow inactivation gradually increases as a function of distance from the soma. Slow inactivation is also frequency and voltage dependent. Higher frequency depolarizations increase both the amount of slow inactivation and its rate of recovery. Hyperpolarized resting potentials and larger command potentials accelerate recovery from slow inactivation. We compare this form of slow inactivation to that reported in other cell types, using longer depolarizations, and construct a simplified biophysical model to examine the possible gating mechanisms underlying slow inactivation. Our results suggest that sodium channels can enter slow inactivation rapidly from the open state during brief depolarizations or slowly from a fast inactivation state during longer depolarizations. Because of these properties of slow inactivation, sodium channels will modulate neuronal excitability in a way that depends in a complicated manner on the resting potential and previous history of action potential firing.

INTRODUCTION

Simultaneous patch-pipette recordings from the soma and dendrites have demonstrated that action potentials are typically initiated in the axon of hippocampal CA1 pyramidal neurons. As well as propagating down the axon to the synaptic terminal, action potentials also propagate actively back into the apical and basal dendrites (Spruston et al., 1995; Callaway and Ross, 1995). Such "back-propagating" action potentials are associated with large dendritic depolarizations and increases in intracellular calcium concentration. This, in turn, may have important physiological implications for the neuron. For example, the depolarization could influence local synaptic processing by resetting the membrane potential (Stuart et al., 1997) or provide an important postsynaptic signal needed for certain types of associative synaptic plasticity (Debanne et al., 1998; Magee and Johnston, 1997; Markram et al., 1997).

One important feature of action potential back-propagation is its activity dependence. During long trains of action potentials, the later spikes are much smaller in amplitude than the earlier spikes and may actually fail to actively propagate (Spruston et al., 1995; Callaway and Ross, 1995). Several hypotheses have been put forth to explain the activity dependence of the attenuation of the back-propagating action potentials, including both long-lasting sodium channel inactivation or some form of activity-induced shunt of the membrane potential (Spruston et al., 1995). Using simplified compartmental models of pyramidal neurons, Migliore simulated each of these hypotheses (Migliore, 1996). He concluded that either mechanism in itself was able to qualitatively reconstruct the experimental findings, and that there were testable predictions for each mechanism.

While empirically investigating the causes of activity-dependent attenuation of action potential back-propagation in CA1 neurons, we found no evidence in support of the shunting hypothesis (Jung et al., 1997). However, we and others discovered that sodium channels in the somata and dendrites of CA1 pyramidal cells do indeed enter a slowly recovering form of inactivation induced by repetitive depolarizations (Colbert et al., 1997; Jung et al., 1997; Martina and Jonas, 1997). The amount of sodium channel inactivation accumulated with increasing numbers of pulses, until it finally reached a steady-state level. In addition, there appeared to be differences between the amounts of inactivation reached in somatic and dendritic channels. We termed this type of inactivation "prolonged" inactivation, to distinguish it from the conventional "fast" inactivation and because its relation to "slow" inactivation was unclear.

To understand how these neurons function, especially in more physiological and complex settings such as neural networks, more accurate data on sodium channel activation and inactivation are needed. This study was motivated by the need to increase our understanding of sodium channel function in CA1 pyramidal neurons, to constrain new models of both sodium channels and neuronal activity. In particular, we wanted to learn how sodium channels differed along the somatodendritic axis and how they might be affected by back-propagating action potentials of different rates and sizes and at different membrane potentials. We also explore the relationship of slow inactivation in CA1 pyramidal cells to that described for other cell types and use

Received for publication 31 July 1998 and in final form 15 October 1998.
Address reprint requests to Dr. Nelson Spruston, Department of Neurobiology and Physiology, Northwestern University, Evanston, IL 60208-3520. Tel.: 847-467-2734; Fax: 847-467-4898; E-mail: spruston@nwu.edu.
HJ and TM contributed equally to this work.

0006-3495/99/02/846/15 $2.00

single-channel models to examine sodium channel gating of slow inactivation.

MATERIALS AND METHODS

Slice preparation

Slices were prepared from 6–10-week-old Wistar rats. No noticeable differences were observed in three patches from 4-week-old animals. The rats were anesthetized with halothane and perfused transcardially with ice-cold artificial cerebrospinal fluid (ACSF). Brains were removed in cold ACSF, blocked for slicing, and placed in the slicing chamber in cold, oxygenated ACSF. Slices were cut into 300-μm sections with either a 752 Vibroslice (Campden Instruments, Loughborough, England) or a Leica VT 1000S tissue slicer (Leica Instruments, Heidelburg, Germany). Slices were then transferred to a holding chamber filled with oxygenated ACSF and stored at 35°C for 30–60 min. Slice quality was stable for ~4 h.

Recordings

Slices were visualized by infrared differential interference microscopy (Stuart et al., 1993) with a fixed-stage microscope (Zeiss Axioscop; Carl Zeiss, Thornwood, NY) and a Newvicon tube camera (Dage-MTI, Michigan City, IN). Glass electrodes (glass type EN-1; Garner Glass, Claremont, CA) were pulled to 4–9 MΩ resistance as measured in the bath (Brown-Flaming P30 puller; Sutter Instruments, Novato, CA), coated with Sylgard to reduce electrode capacitance, and fire-polished. All recordings were made in the cell-attached patch-clamp mode at temperatures of 34–37°C. Seals were made under visual control on either the somata or apical dendrites of hippocampal CA1 pyramidal neurons. Seal resistances were greater than 2 GΩ.

Solutions

ACSF contained (in mM) 125 NaCl, 2.5 KCl, 25 $NaHCO_3$, 1.25 NaH_2PO_4, 1 $MgCl_2$, 2 $CaCl_2$, 25 dextrose. The ACSF was bubbled with a 95% O_2/5% CO_2 gas mixture to oxygenate the solution and provide a pH of 7.4. The pipette solution contained (in mM) 120 NaCl, 3 KCl, 10 HEPES, 2 $CaCl_2$, 1 $MgCl_2$, 30 tetraethylammonium chloride (TEA), and 5 4-aminopyridine (4-AP) (pH 7.4) with NaOH.

Data acquisition and analysis

Voltage-clamp recordings were made using PC-ONE patch-clamp amplifiers (Dagan Instruments, Minneapolis, MN). Currents were filtered at 1 kHz and sampled at 50 kHz. Data were acquired with Macintosh PowerPC computers and an IT-16 interface (Instrutech, Great Neck, NY) and Pulse Control software (Dr. Richard Bookman, University of Miami) written for Igor Pro 3.0 (WaveMetrics, Lake Oswego, OR). Leak and capacitive currents were subtracted online by P/(−4) subtraction. Unless otherwise mentioned, all pulses are 2 ms wide and 50 mV depolarizing in amplitude relative to the resting potential. Patches were held at the resting potential for at least 5 s between pulse trials to prevent accumulation of channels in inactivated states. In some experiments the patches were held hyperpolarized from V_{rest} between trials for at least 5 s. However, there did not appear to be any difference between experiments conducted with either resting potential or hyperpolarized holding potentials. Pulse protocols were also often carried out in a semirandom order so that there would be no stimulus- or time-related artifacts. Currents were examined carefully for signs of rundown over the course of the experiment. If the response to the first pulse was ever less than 75% of the peak current at the start of the experiment, then the trace was rejected. Finally, in many experiments whole-cell configuration was achieved after the experiment, and V_{rest} was determined to vary from −56 to −79 mV (−71 ± 0.7 mV, n = 46 of 177 total patches).

Percent inactivation during a train and recovery at time t after a train were computed as in Jung et al. (1997):

$$\text{Percent inactivation} = \left(\frac{\text{first} - \text{last}}{\text{first}}\right) \times 100\%$$

$$\text{Percent recovery} = \left[\frac{(\text{test} - \text{last})}{(\text{first} - \text{last})}\right] \times 100\%$$

where *first* and *last* are the peak current amplitudes from the respective depolarizing pulses in the train, and *test* is the peak current amplitude at various times t after the train. Amplitude ratios were computed as

$$\text{ratio} = \text{test/first}$$

For all statistical tests, a p-value of less than 0.05 was used as a cutoff for significance. All statistics are reported as mean ± SE. Statistical tests used and p-values of tests are reported in the appropriate figure legends.

Modeling

A kinetic scheme as suggested in Jung et al. (1997) was used as the basis for the models. Simulations of macroscopic currents were obtained by solving the Q matrix (Colquhoun and Hawkes, 1982) with Mathematica (Version 3.0 for Macintosh; Wolfram Research, Champaign, IL) running on a PowerComputing PowerTower Pro 225 (Power Computing, Round Rock, TX). Voltage-dependent rates were created by using Boltzmann-like equations of the form

$$\alpha = A \Big/ \left(1 + \exp\left(\frac{V_{1/2} - V}{k}\right)\right)$$

(see Table 1 for rates and further explanation). To ensure that microscopic reversibility was obeyed in the model, three of the rates were allowed to vary as functions of the other rates. Because of the large number of free parameters in the model, the rates were varied and determined by a trial-and-error approach, to best approximate the empirical data (some

TABLE 1 Parameters used in sodium channel model 2

Transition	C	O	I_{fast}	I_{slow}	
C to		2900	335	0.44	A (s^{-1})
		−28	−47	−48	$V_{1/2}$ (mV)
		5	9	6	k (mV)
		2889	333	0.44	α_0 (s^{-1})
O to	300		3200	1800	
	−10		−47	−30	
	−10		4	6	
	81		3200	1788	
I_{fast} to	—	1		—	
	—	0		—	
	—	−900		—	
	0.0015	0.50		2.0	
I_{slow} to	—	0.47	0.3		
	—	−58	−100		
	—	−10	−30		
	9.7×10^{-9}	0.0014	0.01		

Voltage-dependent rates between states were modeled using Boltzmann-like equations of the form $\alpha = A/(1 + \exp((V_{1/2} - V)/k))$, where A is the maximum rate, V is the membrane potential, $V_{1/2}$ is the potential at which the function equals half the maximum rate, and k is inversely proportional to the steepness of the voltage dependence. In the table, α_0 is the rate at 0 mV. Parameters that best fit the data were determined by a trial-and-error method. To obey microscopic reversibility, some transitions were allowed to vary as functions of the other transition rates (indicated by —).

initial rates taken from Patlak, 1991). The criteria for fitting the experimental data were the percent inactivation induced by a 20-Hz train of pulses, the time constants of recovery after a single short pulse and a train of depolarizing pulses, and the percent inactivation between the first and second pulses in the train (used as an indicator of the rate of entry into prolonged inactivation).

The overall conductance of the model was determined by multiplying the open probability by a linear conductance equal to 150 pS (representing 100 channels with a single-channel conductance of 15 pS; Magee and Johnston, 1995). Currents were then determined by multiplying this conductance by the change in driving force for sodium induced by the voltage protocols, with the reversal potential for sodium set at +66 mV (assuming an internal sodium concentration of 10 mM).

RESULTS

The data in this study were obtained from 177 cell-attached dendritic and somatic recordings. As we have previously shown that these are tetrodotoxin-sensitive currents (Jung et al., 1997), they will be referred to as sodium currents. The pulse protocols used were designed to mimic the types of depolarizations that the channels would experience during action potential firing. We found no noticeable difference between dendritic and somatic resting potentials, which is consistent with previous work (Spruston et al., 1995).

Prolonged inactivation increases with distance from soma

We and others have previously reported that the amount of prolonged inactivation that occurs during a train of voltage commands is significantly different for sodium channels of the apical dendrites than for somatic sodium channels (Colbert et al., 1997; Jung et al., 1997). However, it was unknown whether there was a smooth transition between somatic and dendritic channels, or if there was a more discrete jump in prolonged inactivation of the channels. To better determine this transition, recordings of prolonged sodium channel inactivation were made from somata and apical dendrites at distances of 10–300 μm from the soma. Fig. 1 *B* shows the percentage inactivation induced by a 20-Hz train of depolarizing pulses plotted as a function of recording location. Although there is some scatter to the distribution, the overall shape is a smoothly increasing function that begins to plateau at ~200 μm. The data were fit by a single exponential with a distance constant of 126 μm. In contrast to the inactivation data, Fig. 1 *C* shows that there is no relationship between distance and recovery from inactivation. We also found, in accordance with the results of Magee and Johnston (1995), no evidence for a nonuniform distribution of sodium channel density (data not shown). We used the distance information to constrain the subsequent experiments by making dendritic recordings between 100 and 180 μm from the soma (with the majority occurring between 120 and 160 μm). The amount of inactivation induced by a 20-Hz train is ~60% in this region, which is enough to be readily visualized and analyzed.

Recovery from prolonged inactivation has an exponential time course

Any type of long-lasting inactivation of sodium channels can affect the ability of a neuron to fire action potentials and therefore could affect how the neuron will integrate subsequent inputs to produce an output. Because the prolonged inactivation we have described could influence the availability of sodium channels supporting action potential generation or back-propagation into dendrites, it was important to determine the time course of recovery from this activity-induced inactivation. Fig. 2 *A* shows an example of the recovery time course from a 20-Hz train of depolarizing pulses in a dendritic recording 120 μm from the soma. Eighteen single traces have been overlaid to demonstrate the time course. While 50% of the inactivated current recovered in less than 1 s, the remaining inactivated current in this patch required 4.5 s to fully recover. The summary data in Fig. 2 *B* show that, on average, recovery is a slow process that appears to be exponential in nature. Fitting the data with a single exponential revealed a time constant of 863 ms. This value is several hundred times greater than the time constant usually measured for recovery from the typical "fast" inactivation. It is also interesting to note that there appears to be a slight potentiation of the sodium current for recovery times greater than 4 s. As there does not appear to be a relationship between recovery and recording site (see Fig. 1 *C*), these results should apply to sodium channels at all somatic and dendritic locations.

Amount of prolonged inactivation and its recovery are frequency dependent

Because sodium channel inactivation, and therefore neuronal excitability, may be very different depending on a neuron's previous firing history, we investigated the effects of a range of physiological firing frequencies on induction and recovery from prolonged inactivation. Fig. 3 *B* shows that the amount of prolonged inactivation during a train increased with increasing frequency in both dendritic and somatic sodium channels. The rate of accumulation in the prolonged inactivated state also increased with frequency. During a 20-Hz train of pulses, the average accumulation had a time constant of 124 ms; for a 50-Hz train, the time constant was 51 ms (data not shown; see Fig. 3 *A* for individual examples). The recovery data shown in Fig. 3 *B* indicated that increasing frequency leads to a statistically significant faster recovery from prolonged inactivation in dendritic sodium channels. These results are surprising because a single prolonged inactivated state cannot lead to different recovery time courses, even after entry at different rates. Therefore, these data suggest the possible existence of at least one other prolonged inactivated state with a faster recovery, which is induced preferentially by higher frequency stimuli (see Discussion).

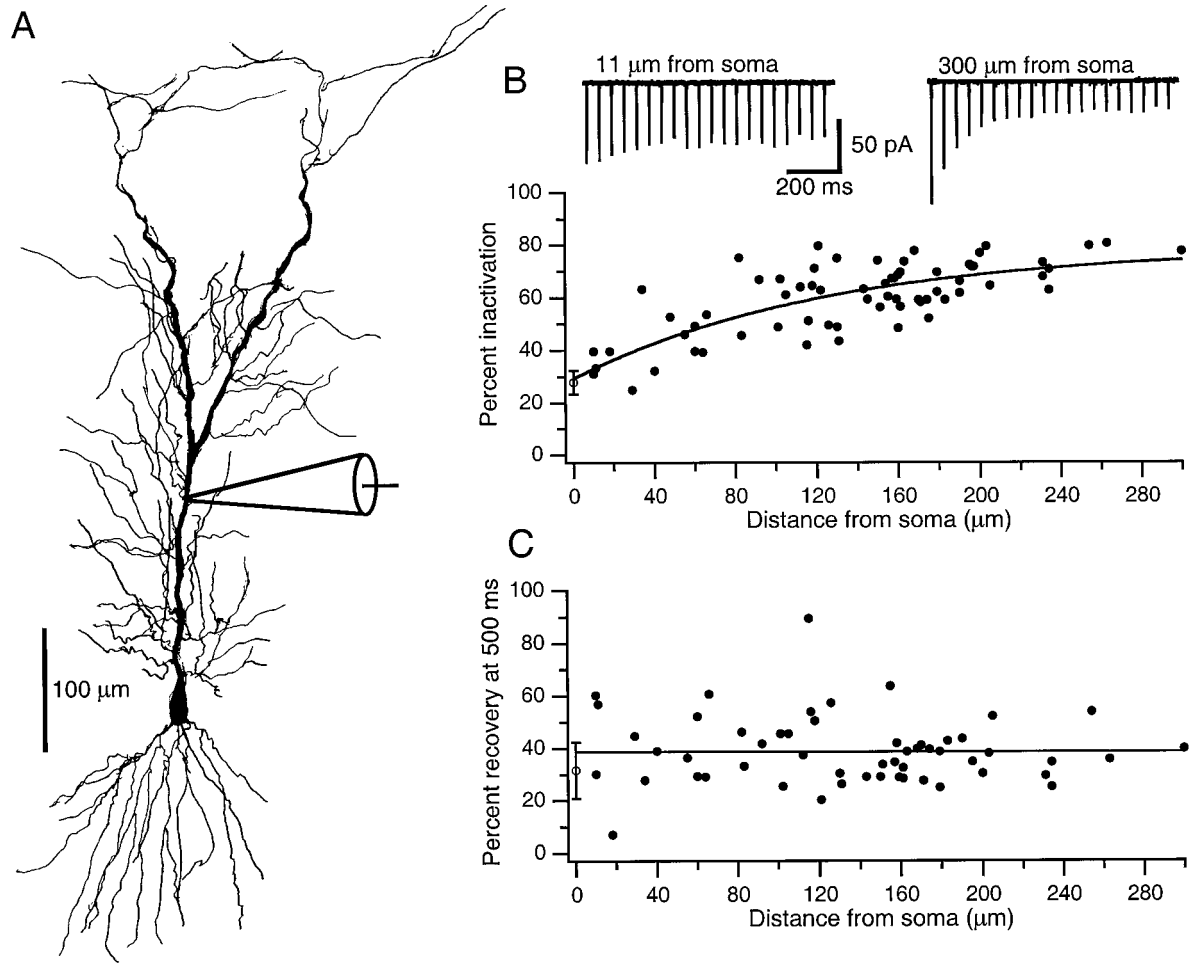

FIGURE 1 Prolonged inactivation but not recovery of sodium currents depends on recording location. (*A*) A camera lucida drawing of a representative CA1 pyramidal cell. Recordings were made from somata or primary apical dendrites between 10 and 300 μm from the soma. (*B*) Percentage inactivation and (*C*) percentage recovery at 500 ms after a 20-Hz train of pulses plotted against recording location. ●, Dendritic recordings (*B*, $n = 67$ cells; *C*, $n = 54$ cells). ○, Somatic average values (*B*, $n = 7$ cells; *C*, $n = 4$ cells; error bars are SE). The curve in *B* is fit by a single exponential function with a distance constant of 126 μm. The line in *C* is a linear regression through the data (slope $= -9.2 \times 10^{-4}$, $r^2 < 3 \times 10^{-5}$). Somatic data were weighted appropriately. Insets in *B* are averaged sodium currents from dendritic patches at 11 μm (average of four sweeps) and 300 μm (average of nine sweeps) from the soma; the scale bar is the same for each. Command pulses were 2-ms-wide, 50-mV depolarizations.

Recovery from prolonged inactivation is voltage dependent

Considering that the membrane potential could fluctuate considerably in vivo (Soltesz and Deschenes, 1993; Kamondi et al., 1998b), it is important to determine whether the degree of prolonged inactivation and recovery from prolonged inactivation are voltage dependent. While examining the effects of holding potential, we varied the command step size to reach the same absolute membrane potential for all holding potentials (Fig. 4 *A*). In this way, we tried to eliminate the possibility that differences in driving force or absolute command potential might confound the effects of holding potential. As shown in Fig. 4 *B*, holding potential had only a small effect on entry into prolonged inactivation in dendritic sodium channels. Holding dendritic patches at potentials hyperpolarized by more than 10 mV to the resting potential led to a small but statistically significant decrease in the amount of prolonged inactivation. However, holding dendritic patches at depolarized potentials did not affect prolonged inactivation, nor was there any statistically significant effect of holding potential on inactivation of somatic sodium channels.

The effect of holding potential on recovery from prolonged inactivation is more dramatic (Fig. 4 *C*). Holding potentials hyperpolarized 10 mV or more from the resting potential promoted recovery of dendritic sodium currents significantly, whereas depolarized potentials had no effect on recovery from prolonged inactivation. The effect of holding potential on somatic recovery was not statistically significant, but displayed a trend similar to the effect on dendritic recovery. Although hyperpolarized potentials did not cause large differences in prolonged inactivation from the resting potential, they could, because of the enhancement of recovery, change the availability of sodium chan-

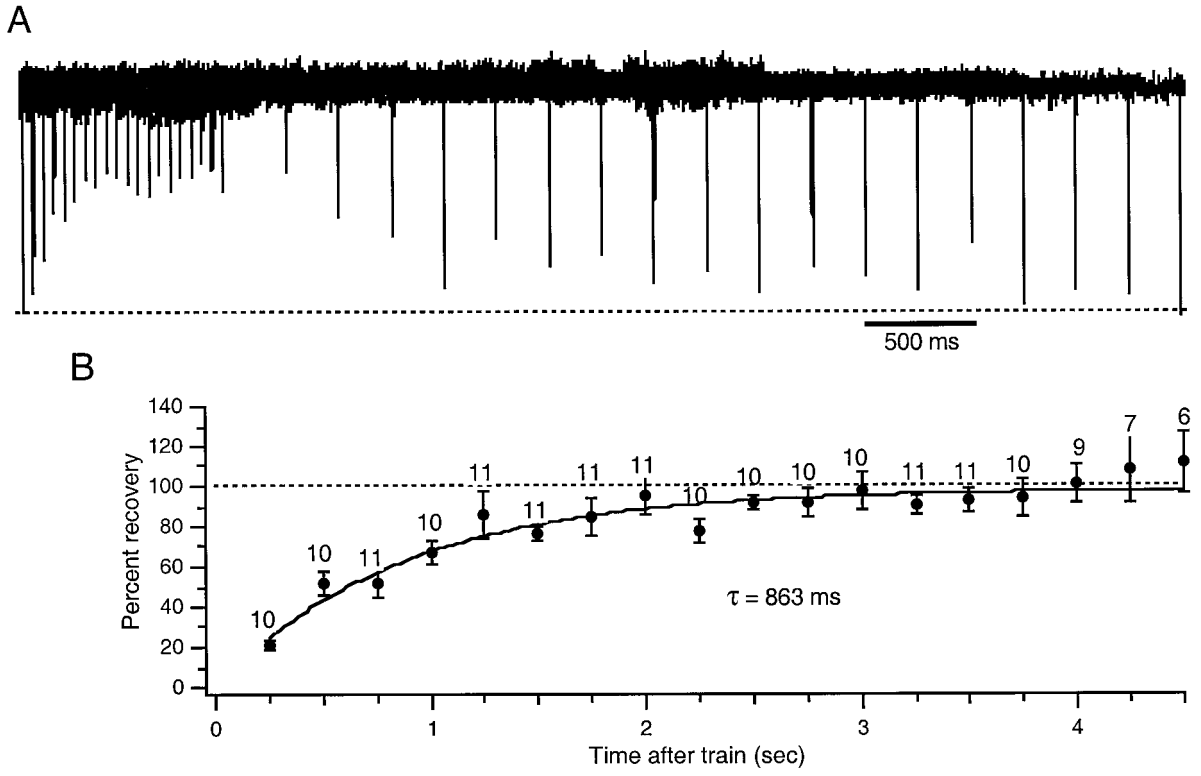

FIGURE 2 Time course of recovery of dendritic sodium channels from prolonged inactivation induced by a 20-Hz train. (*A*) Eighteen overlaid traces from the same dendritic patch demonstrating the recovery time course. Each trace is a single trial, which includes a 20-Hz train followed by a recovery test pulse at a variable interval. Each trace is normalized to the current of the first response in the train (peak ranged from 58 to 100 pA) to better demonstrate the recovery time course and to control for sweep-to-sweep variation. This particular set was from a dendritic recording 120 μm from the soma and had an average inactivation of 71%. Note that the inactivated sodium current does not fully recover until 4.5 s after the train. (*B*) Summary data for recovery of dendritic sodium channels from prolonged inactivation. Numbers of cells tested at each recovery time point are indicated above each data point, and error bars are the SE. The solid curve is a single exponential fit of the data, having a recovery time constant of 863 ms. The dashed line at 100% recovery is for reference. Command pulses were 2-ms-wide, 50-mV depolarizations.

nels considerably. These results suggest that the local changes in membrane potentials caused by spatially restricted inhibitory or excitatory synaptic inputs could modulate the availability of dendritic and somatic sodium channels.

The amplitude of dendritic action potentials is usually smaller than those at the soma and is highly variable, depending on location and prior activity (Golding and Spruston, 1998; Spruston et al., 1995). Varying the size of voltage could therefore be another way to affect the degree of prolonged inactivation and to modulate the excitability of dendrites differentially from that of the soma. In this regard, we examined the effect of various command step sizes on the induction of prolonged inactivation and its recovery at the resting potential. As shown in Fig. 5 *A*, different step sizes did not have any effect on the degree of prolonged inactivation in dendritic or somatic channels. Surprisingly, however, the recovery from prolonged inactivation increased significantly as command step size was increased in dendritic and somatic patches (Fig. 5 *B*). This result is unexpected if we assume only one prolonged inactivation state. Therefore, it provides further evidence of more than one prolonged inactivation state (see Discussion). In the experiments shown in Fig. 5, *A* and *B*, the size of the 20-Hz train and the test pulse 500 ms after the train were the same. To confirm that the enhancement of recovery by large command potentials is not due to the size difference of the test command potential, in the experiment in Fig. 5 *C*, the same size test pulse (70 mV for both) was preceded by different size trains. It is clear that prolonged inactivation induced by the larger command potential had a faster recovery, even with a constant test pulse. The effect of step size on recovery from prolonged inactivation is similar in somata and dendrites; the effect of step size could cause the availability of sodium channels in dendrites and somata to differ, because action potential amplitudes generally are not equal in these regions (Golding and Spruston, 1998; Spruston et al., 1995).

Prolonged inactivation is induced by a single brief depolarization

We have shown previously that prolonged inactivation is distinct from conventional fast inactivation of sodium channels (Jung et al., 1997). However, the exact difference in recovery time course of these two types of inactivation has not been investigated in CA1 pyramidal cells. To examine the time course of recovery more closely, a two-pulse pro-

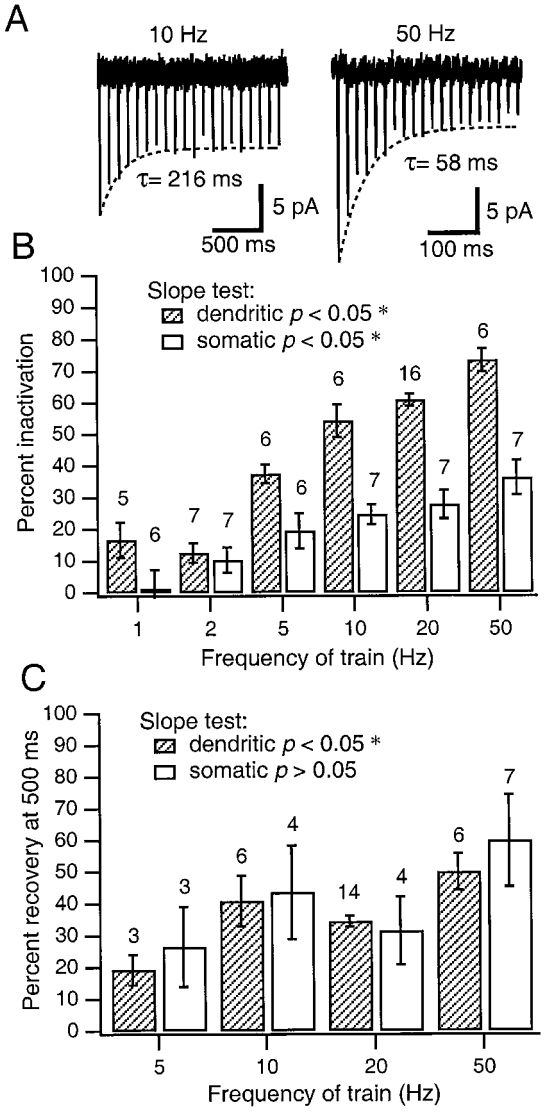

FIGURE 3 Effects of stimulus frequency on prolonged inactivation and recovery from prolonged inactivation. (*A*) Current responses to 10- and 50-Hz depolarizing trains demonstrating frequency effects on prolonged inactivation. The 50-Hz train has greater inactivation (81% compared to 49% at 10 Hz) and a faster rate of accumulation of prolonged inactivation. Traces are averages of four responses, both from the same dendritic patch (151 μm from the soma). (*B*) Summary data of percent inactivation during a train of the given stimulus frequency. Dendritic (□) and somatic (▨) percent inactivation increases with pulse train frequency. Linear regressions of both somatic and dendritic data have slopes that are significantly different from zero (dendritic slope 1.15; somatic slope 0.56; Student's *t*-test that slopes do not equal zero: dendritic, $p < 7 \times 10^{-10}$; somatic, $p < 5 \times 10^{-5}$). Numbers of cells tested at each frequency are indicated above each bar, and error bars are the SE. (*C*) Summary data of recovery from inactivation induced by a train of the given stimulus frequency. Dendritic (▨) but not somatic (□) percent recovery at 500 ms increases with pulse train frequency. Linear regression of the dendritic data has a slope value that is significantly different from zero (dendritic slope = 0.44; Student's *t*-test that slopes do not equal zero: dendritic, $p < 0.01$). Command pulses were 2-ms-wide, 50-mV depolarizations. Numbers of cells tested at each frequency are indicated above each bar, and error bars are the SE.

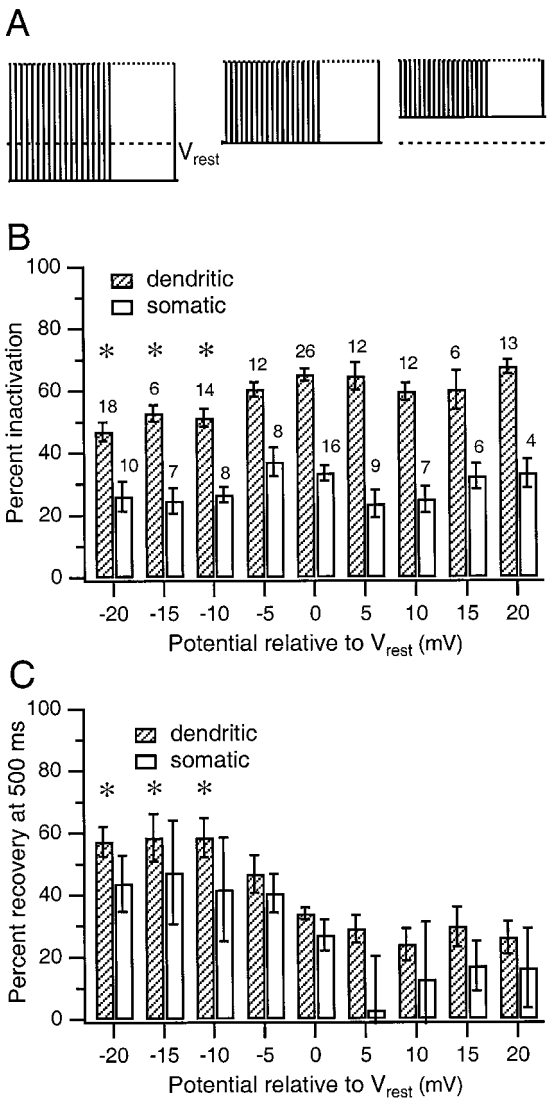

FIGURE 4 Effect of holding potential on prolonged inactivation and recovery from prolonged inactivation in dendritic (▨) and somatic (□) currents. (*A*) Protocol used for *B* and *C*. Control data were obtained from the resting potential (V_{rest}), and the command step size was varied according to the holding potential to reach the same absolute membrane potential (indicated by the *upper dotted line*) as the control. (*B*) Percent inactivation at the end of a 20-Hz train of 2-ms depolarizations in dendritic and somatic channels is plotted for different holding potentials. Numbers of cells tested at each holding potential are indicated above each bar, and error bars represent SE. A one-way ANOVA on somatic data supports the null hypothesis that there is no significant difference among somatic groups. Holding dendritic patches at depolarized potentials does not affect prolonged inactivation. Statistical tests showed that dendritic data held at more than 10 mV hyperpolarized to the resting potential differed significantly from the control (*, one-way ANOVA with Tukey's *t*-test, $p < 0.001$). (*C*) Recovery from prolonged inactivation in dendrites and somata plotted against various holding potentials. Data were collected from the same cells as in *B*. A one-way ANOVA shows that there is a significant difference among the dendritic groups, whereas no significant difference appears among the somatic groups. A Tukey's *t*-test was performed for dendritic groups and showed that holding potentials hyperpolarized 10 mV or more from the resting potential promoted recovery significantly (*, $p < 0.005$).

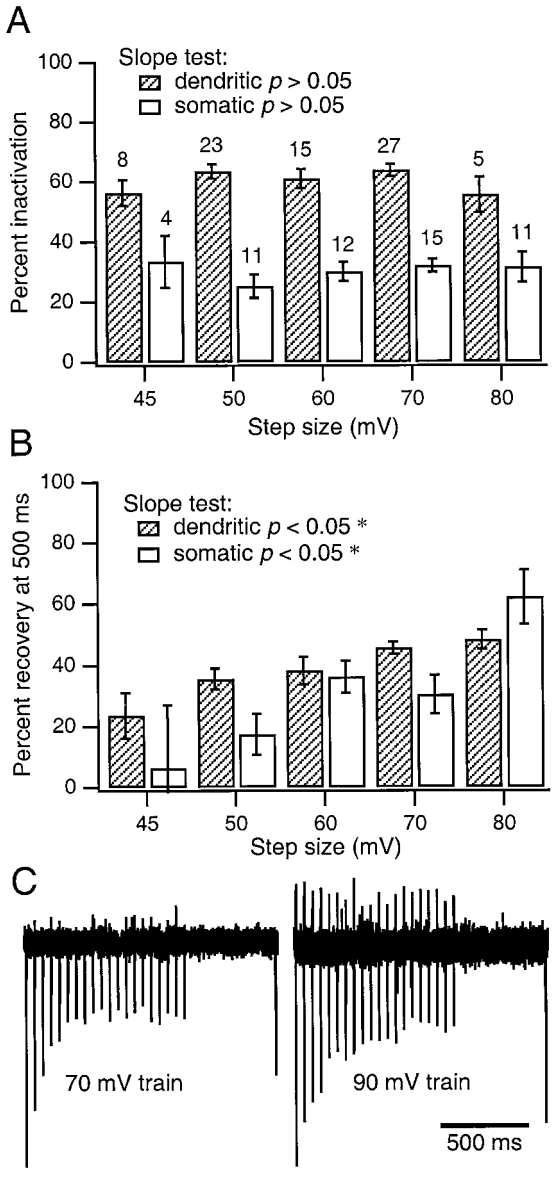

FIGURE 5 Effect of command potential on the prolonged inactivation and its recovery in dendrites (▨) and somata (□). All data were collected at the resting potential. (*A*) Prolonged inactivation in dendrites and somata induced by 20-Hz trains of 2-ms depolarizations of different sizes. Numbers of cells tested at each command potential are indicated above each bar, and error bars represent SE. Linear regression performed shows that slopes are not significantly different from zero in both dendrites and somata (somatic $r^2 < 0.02$, dendritic $r^2 < 5 \times 10^{-4}$). (*B*) Recovery from prolonged inactivation induced by different sizes of command potential. Same cells as in *A*. Linear regression of the data indicates that slopes are significantly different from zero in both dendrites (slope = 0.6, $p < 0.001$) and somata (slope = 1.3, $p < 0.001$). (*C*) Effect of command potential size in the train on the recovery. *Left*, Current evoked by a 70-mV step during a train with a test pulse. *Right*, Current evoked by a 90-mV step during a train with a 70-mV test pulse. Both traces are the average of four responses from the same dendritic patch (140 μm from the soma) and are scaled by its first peak (23 and 30 pA, respectively) in the train for better comparison of its recovery.

tocol with brief depolarizations was used. Fig. 6 *A* shows, in a typical patch, the recovery time course from inactivation induced by a single 2-ms depolarizing pulse, and Fig. 6 *B* shows the pooled data from 22 cells. The group data were fitted by a double exponential. Although there were points that deviated in the short interpulse intervals, the biphasic recovery had a fast time constant of 2.0 ms and a slow time constant of 1.2 s. This result demonstrates that a significant fraction of sodium channels enter a slowly recovering inactivated state, even after a single brief depolarization.

Prolonged inactivation and slow inactivation

"Slow" inactivation of sodium channels has been reported by many investigators in various preparations (Narahashi, 1964; Rudy, 1978; Fleidervish et al., 1996). It has typically been induced by a long, sustained depolarization (>500 ms), because its onset and recovery were known to occur on a several-second time scale (Fleidervish et al., 1996; Featherstone et al., 1996; Ruff et al., 1988). In some cases, slow inactivation has been reported to be inducible by shorter (~20–350 ms) depolarizations (Starkus and Shrager, 1978; Rudy, 1981; Quandt, 1988); however, it is not known whether slow inactivation can be induced by more physiological stimuli, such as even briefer depolarizations, or trains of depolarizations. To test whether the biophysical identity of inactivation induced by brief depolarizations is the same as slow inactivation induced by longer depolarizations, a series of experiments were performed.

First, the rate of entry into the slow inactivation was examined by varying the duration of prepulses (Fig. 7). The amount of inactivation increased as a function of prepulse duration, as shown by the superimposed current traces in Fig. 7 *A*. The inactivation process was well fit by a single exponential, and the time constant for the entry into slow inactivation was 390 ms (Fig. 7 *B*). Note, however, the additional fast component of entry, as even the shortest prepulses exhibit ~20% inactivation. For the subsequent experiments, we chose a 500-ms prepulse duration, as this induced near-maximum slow inactivation. Fig. 8 shows the time course of recovery from inactivation induced by a long depolarizing prepulse. The test pulse duration (2 ms) and step size (70 mV) were the same as those in Fig. 6, to facilitate a direct comparison of the recovery time course for inactivation due to long or short prepulses. Fig. 8 *A* demonstrates the recovery time course from inactivation induced by a long (500 ms) depolarization in a typical dendritic patch. The pooled data from nine dendritic patches are shown in Fig. 8 *B* and fit with a double exponential. The fast time constant was not considered to be meaningful because the shortest interpulse interval used to obtain the data (Δt = 40 ms) was longer than this fast time constant. The slow time constant of this double exponential was very similar to the slow time constant in Fig. 6 (1.3 s versus 1.2 s), suggesting that prolonged inactivation and slow inactivation may be the same phenomenon.

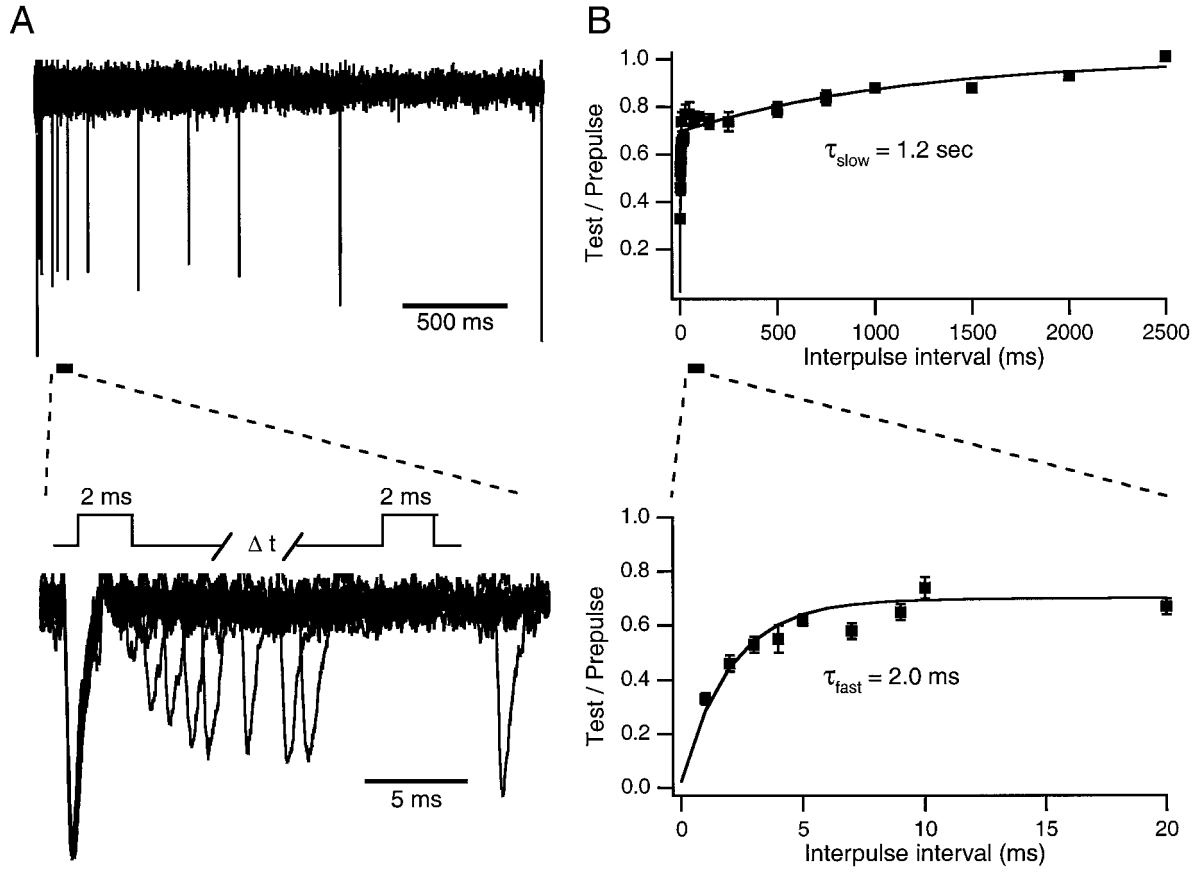

FIGURE 6 Time course of recovery of dendritic sodium channels from inactivation induced by a single brief depolarization. (*A*) Eighteen overlaid traces from the same dendritic patch demonstrating the recovery time course from inactivation caused by a brief depolarizing prepulse. The lower traces are expansions of the first 20 ms of the upper graphs. The diagram above the lower traces shows the two pulse protocol used to obtain the recovery time course. Each pulse is a 2-ms-long, 70-mV step from the resting potential separated by a variable interpulse interval (Δt) and is the average of two to nine raw traces, scaled by its first peak (ranging from 13 to 18 pA) for the better demonstration of recovery. This particular set was recorded 140 μm from the soma. (*B*) Group data for the recovery time course. Ratio of the first to the second peak current is plotted as a function of interpulse interval (Δt) and fit with a double-exponential function, shown as a solid line. The lower graph is the enlargement of the first 20 ms of the upper graph. Each point is the average of more than seven cells; the error bars indicate SE. τ_{slow} and τ_{fast} represent time constants for recovery from slow and fast inactivation, respectively.

In the third experiment, we tested the above hypothesis by comparing the amount of inactivation that occurs during a train of pulses with and without a long depolarizing prepulse. We reasoned that if the two processes are distinct, then it should be possible to see both slow inactivation and further inactivation that occurs over the course of the train. A 1-s, 70-mV depolarizing prepulse was used to induce slow inactivation of the sodium channels, followed by the train protocol. A 40-ms interval between the long pulse and the train allowed for recovery from fast inactivation. In Fig. 9 *A*, a 20-Hz train of pulses was compared with and without a prepulse. Without the prepulse the sodium current inactivated over the course of the pulse train until a steady state was reached. When the prepulse was given before the train, the current was initially smaller than the steady state reached during the control train and actually recovered over the course of subsequent depolarizing pulses, until it finally reached a level nearly equal to the control steady state.

A possible explanation for the observed recovery of the channels during the 20-Hz train after the prepulse is that the interpulse interval was long enough (48 ms) to allow a slight recovery of some sodium channels from the slow inactivation state. To control for this, we increased the frequency to 50 Hz. Fig. 9 *B* shows that no further inactivation occurred over the course of the train after the prepulse. Rather, the inward currents stayed relatively constant (with some initial recovery toward the control steady-state level) and smaller than the control steady state. These data, together with the results from the experiments of Figs. 6 and 8, indicate that the "prolonged" inactivated and "slow" inactivated states are indistinguishable in the experiments that we have conducted (see Discussion for details).

Modeling of slow and fast inactivation

To test further whether a distinction should be made between prolonged inactivation and slow inactivation, we attempted to simulate the experimental data by using a model with a single slow inactivation state. Two possible

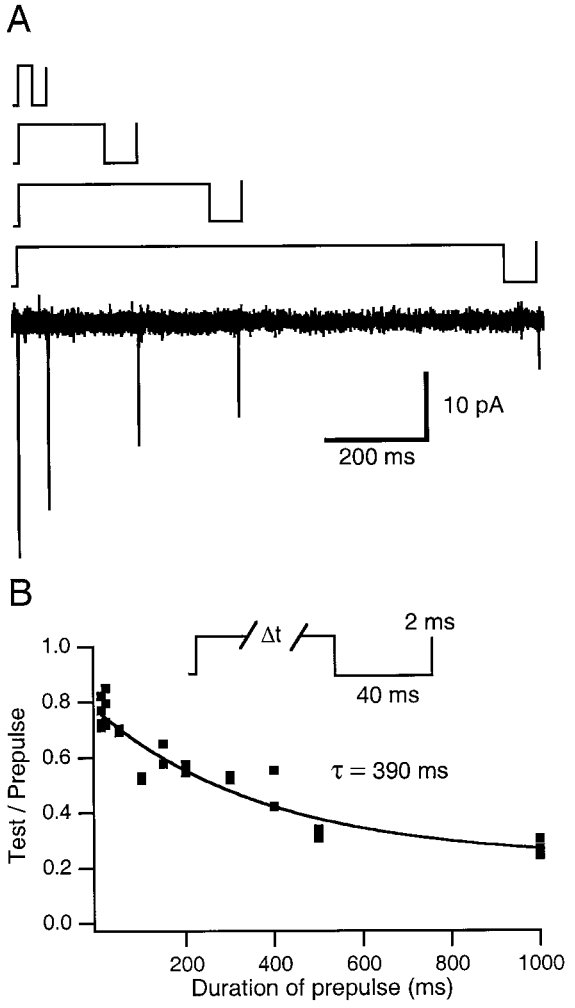

FIGURE 7 Slow entry into inactivation in dendritic sodium channels. (*A*) The top four traces indicate the voltage protocols used for the four superimposed responses below. The duration of each prepulse was varied, and the amount of inactivation was measured by the 2-ms test pulse after a 40-ms recovering interval (70-mV step). Each trace is the average of four to six responses collected in the same dendritic patch (131 μm from the soma). (*B*) Pooled data for the time course of entry into inactivation. The ratio of test to prepulse peak current is plotted as a function of prepulse duration (Δt was varied from 10 ms to 1 s) and fitted with a single exponential shown as a solid line. Data were collected from four cells, and each point represents the average of four to six responses in a dendritic patch. τ is the time constant for induction of slow inactivation.

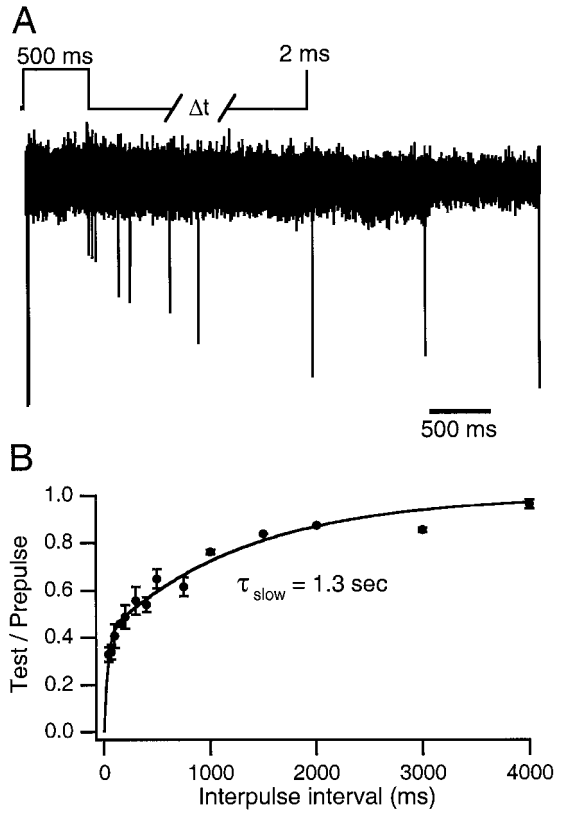

FIGURE 8 Time course of recovery of dendritic sodium channels from inactivation induced by a long depolarization. (*A*) Ten overlaid traces from the same dendritic patch, demonstrating the recovery time course from inactivation caused by long depolarizations. The protocol used is shown at the top of the traces. The duration of prepulse and test pulses was 500 ms and 2 ms, respectively, separated by a variable recovery time (Δt). Each trace is the average of two to six traces collected in one dendritic patch (140 μm from the soma) and scaled by its first peak (ranging from 14 to 24 pA). (*B*) Group data for the recovery time course. The ratio of first to second peak current is plotted as a function of interpulse interval (Δt) and fitted with a double-exponential function, shown as a solid line. Each point is the average of two to nine cells; the error bars indicate SE. τ_{slow} is the slow inactivation time constant. Error bars that are not visible are smaller than the symbol.

channel gating schemes are shown in Fig. 10. These gating schemes have been depicted in such a manner as to provide information about connections between the channel states and how the transitions are likely to occur. The rate constants of all transitions are voltage dependent, with transitions moving toward the top of the figure (in the direction of the *center arrow*) promoted by depolarization and transitions moving toward the bottom of the figure promoted by hyperpolarization (see Table 1 and Materials and Methods). These diagrams are scaled in the vertical direction proportional to the free energy difference between the closed state and the other states at 0 mV and 37°C (see legend of Fig. 10 for details). In general, the parameters choosen for the rate constants were varied in a trial-and-error approach, so that the resulting rates lead to currents with the appropriate kinetics for both fast and slow inactivation.

We originally suggested a simple four-state model with the gating scheme shown in model 1 of Fig. 10 *A* (Jung et al., 1997). The four states, closed (C), open (O), fast inactivated (I_{fast}), and slow inactivated (I_{slow}), are all linked, allowing the I_{slow} state to be reached from any other state (see also Ruff, 1996). There are two particularly important features of this model. First, the I_{slow} to C transition is enhanced by hyperpolarization, which explains the experimental observation that hyperpolarization accelerates recovery (Jung et al., 1997; Colbert et al., 1997). Second, the I_{slow} to I_{fast} transition is enhanced by depolarization, which we originally proposed as a possible explanation for the large

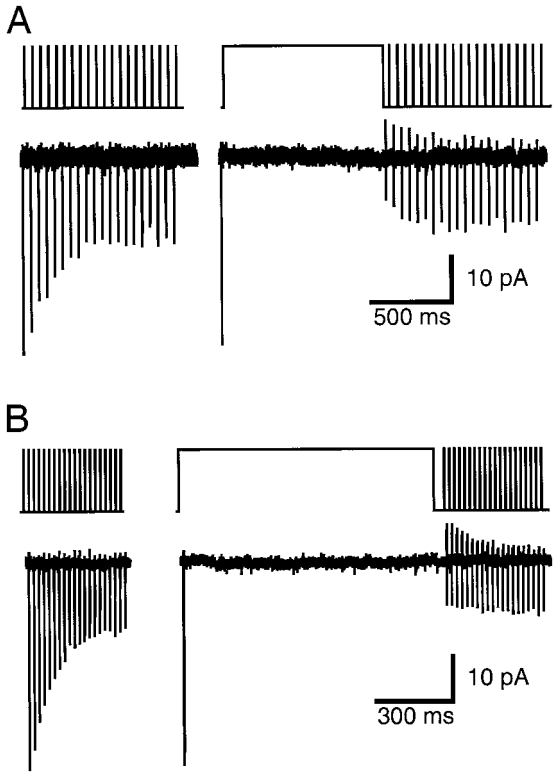

FIGURE 9 Long depolarizing prepulses prevent further prolonged inactivation of dendritic channels. Pulse protocols are shown above each set of traces. (*A*) Occlusion of prolonged inactivation at 20 Hz. The control 20-Hz train shows 57% inactivation (*left*), but after a 1-s-long, 70-mV depolarizing pulse (*right*), the current shows some recovery from the effects of the prepulse. The control and prepulse traces each are the averages of three responses. (*B*) Occlusion of prolonged inactivation at 50 Hz. The control 50-Hz train has 68% inactivation (*left*) and slight recovery after a 1-s-long, 70-mV depolarizing prepulse (*right*). Control and prepulse traces each are the averages of eight responses. Recordings in *A* and *B* were from the same patch, 160 μm from the soma.

steady-state current observed in somatic patches (Jung et al., 1997).

As patches may contain both slowly inactivating and non-slowly inactivating channels, those patches that have sodium currents that demonstrate the greatest inactivation are likely to contain a more homogeneous population of slowly inactivating channels (see Discussion). We therefore attempted to model the most extreme cases of slow inactivation recorded from dendritic patches stimulated at 20 Hz (indicated by the *dashed lines* in Fig. 10). As can be seen from the dashed line in Figure 10 *B* (*left*), the rate of accumulation of slow inactivation, as well as the amount of inactivation at the end of the train, is similar to that from the dendritic channel data. In addition, the recovery time constant for this model is reasonably close to the empirical data (model 1 recovery $\tau = 805$ ms; compare to 863-ms recovery τ of Fig. 2). This model also predicts the acceleration of recovery from slow inactivation by a hyperpolarizing pulse given during the recovery period, similar to that seen in Jung et al. (1997) (data not shown; percentage recovery after 30-mV hyperpolarizing pulse for 452 ms: 87 ± 7%, $n = 5$; model 1 predicts 101%).

A second simple model was also tested (model 2 of Fig. 10 *A*). Like the first model, transitions can occur between all four states, and hyperpolarization leads to an increased recovery from slow inactivation by increasing the I_{slow} to C transition. Model 2 differs, however, in that depolarization promotes entry into I_{slow} from I_{fast} instead of the reverse. Even with this different transition scheme, this second model is able to reproduce the basic findings in a manner comparable to that of model 1 (Fig. 10 *B*, *right*). Model 2 nearly matches the empirical data in both the rate of accumulation and the amount of steady-state current during a 20-Hz train. The rate of recovery from slow inactivation induced by the train is approximately the same as the empirical data and model 1 (model 2 recovery $\tau = 800$ ms) and can be accelerated by a hyperpolarizing pulse (model 2 predicts 102%).

The experiment that best distinguishes between the two models is shown in Fig. 10 *C*, in which we simulate the prepulse experiment of Fig. 9. The responses of each model to this protocol are shown in the upper panels of Fig. 10 *C*. Unlike the results from Fig. 9, model 1 exhibits considerable slow inactivation during a train even after a 1-s prepulse. Model 2, however, qualitatively demonstrates the behavior of the experimental data, showing recovery of the current during the train of depolarizing pulses (compare to Fig. 9 *A*). This indicates that model 2 may be a more accurate representation of the channel gating than our original model (model 1).

The underlying mechanism that leads to the differences between the two models is seen in the middle panels of Fig. 10 *C*, in which the fraction of channels in both the I_{fast} and I_{slow} states are plotted over the course of the prepulse experiment. Model one enters the I_{fast} state more readily than the I_{slow} state, and $f(I_{slow})$ remains smaller throughout the long prepulse. Model 2 initially enters the I_{fast} state preferentially, but $f(I_{fast})$ begins to decrease after ~2 ms. Simultaneously, $f(I_{slow})$ increases and eventually crosses over the $f(I_{fast})$ curve at ~200 ms, reflecting the tendency of the model to leave the I_{fast} state for the I_{slow} state during depolarizations. Eventually, a large $f(I_{slow})$ value is reached, which actually decreases during the train of short pulses. Both models also show an initial rapid transition from the open state to both the I_{fast} and I_{slow} states, which can be better seen in the bottom panels of Fig. 10 *C*. This suggests that dendritic sodium channels could reach a "decision point" at O, in which the majority will enter I_{fast}, but some proportion could also enter I_{slow}. This direct entry into I_{slow} is largely responsible for the first time constant observed when the I_{slow} curve is fit by a two-exponential function ($\tau_1 = 0.52$ ms, $A_1 = -0.34$; $\tau_2 = 459$ ms, $A_2 = -0.68$). The more direct route to I_{slow} from O is probably particularly important in vivo, where fast transient depolarizations (such as action potentials) are much more likely to occur than prolonged large depolarizations. The direct O-to-I_{slow} transition also indicates that at least some of the observed

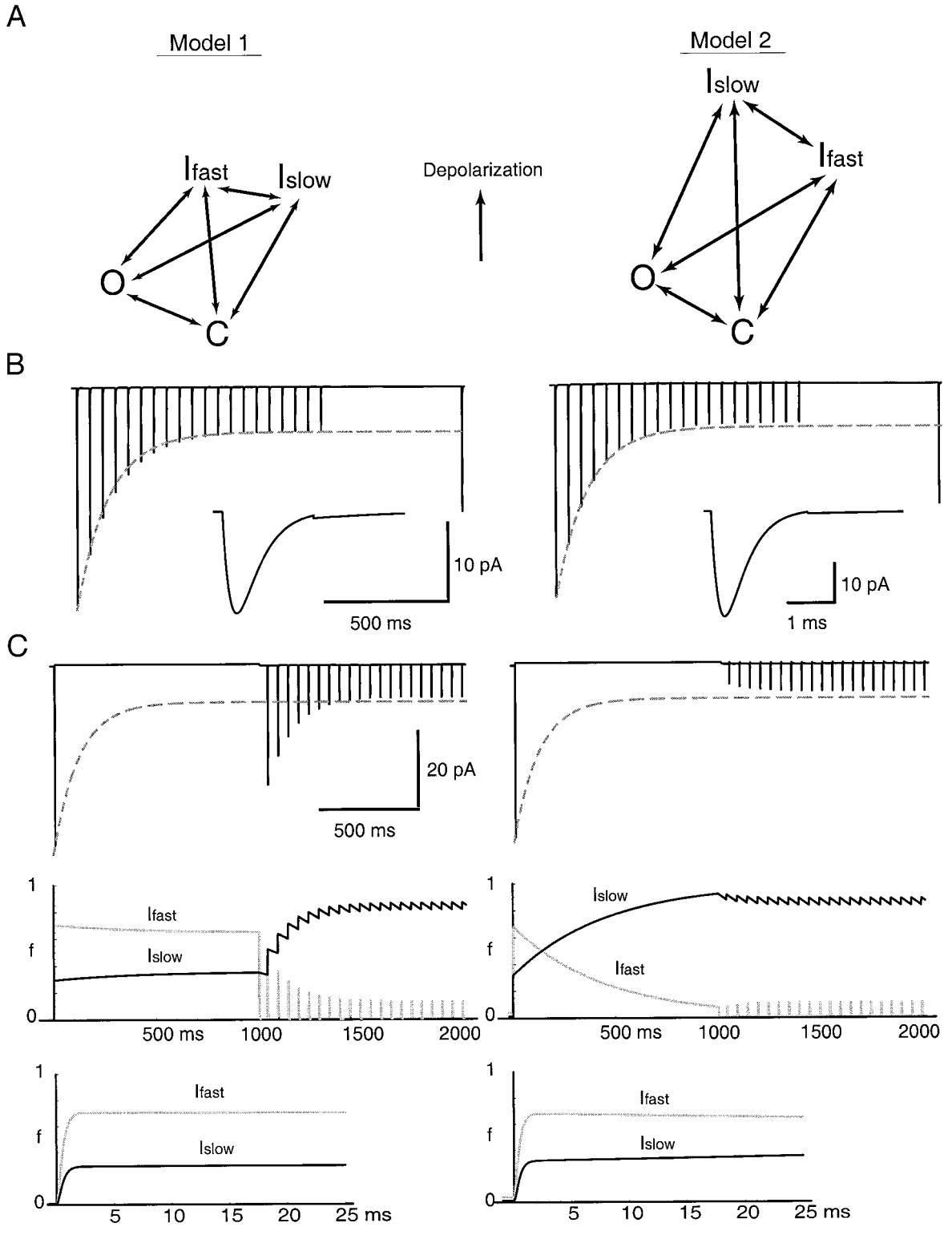

FIGURE 10 A simple gating model can reproduce many of the experimental results. (*A*) The original proposed model, from Jung et al. (1997) (model 1), and a variant of the model (model 2). C is closed, O is open, I_{fast} is fast inactivated, and I_{slow} is slow inactivated. The direction of the arrows is such that an upward direction is a transition promoted by depolarization, and a downward direction is a transition promoted by hyperpolarization. Both models are scaled in the vertical direction by the change in free energy between C and the other states at 0 mV, such that the length of the center vertical arrow represents −5 kJ/mol. Hence the diagram provides information only about the relative proportions in various states at equilibrium. For actual rates, consult Table 1. The scaling was done using the equation $\Delta G = -RT \ln(K)$, where ΔG is the free energy difference relative to C, R is the gas constant, T is the temperature, and K is the ratio of the forward and backward rate constants (at 0 mV). Note that the models differ in the location of I_{slow} relative to I_{fast}. (*B*) Models 1 and 2 (*left* and *right*, respectively) both demonstrate induction of slow inactivation during simulations of a 20-Hz train of depolarizing pulses. The recovery pulse shown is 500 ms after the end of the train. Both models recover from the inactivation on a time course similar to that of the empirical

"fast" inactivation of sodium channels actually may be direct entry of channels into a slow inactivated state from the open state. That model 2 simulates the prepulse experiment better than model 1 suggests that transitions from the fast inactivated state into the slow inactivated state occur during prolonged depolarizations and that this is a better model of the gating mechanism than our original model. These results also suggest that a single slow inactivated state is sufficient to explain the majority of our experimental results (but see Discussion).

DISCUSSION

We investigated the properties of prolonged inactivation, which has been shown to mediate activity-dependent attenuation of back-propagating action potentials in dendrites of CA1 pyramidal cells. Because we were interested in the more physiological aspects of prolonged inactivation, our protocols were designed to mimic physiologically realistic stimuli and conditions. The major findings of this study are as follows: 1) prolonged inactivation of sodium channels increases along the somato-dendritic axis, but reaches a plateau beyond ~200 μm; 2) induction and recovery from prolonged inactivation in dendritic channels increase as a function of stimulus frequency; 3) recovery from prolonged inactivation in dendritic and somatic channels increases as a function of command voltage; 4) recovery of dendritic sodium channels after repetitive depolarizations is accelerated at hyperpolarized holding potentials but not changed at depolarized holding potentials (relative to V_{rest}); 5) prolonged inactivation in dendritic channels can be induced by a single brief depolarization; and 6) most of the data can be simulated by a simple single-channel model that has a single slow inactivation state.

Slow inactivation versus prolonged inactivation

Slow inactivation of sodium channels, which is distinct from conventional fast inactivation, has been studied in a variety of preparations, including skeletal muscle, squid giant axon, and neocortical neurons (Rudy, 1978; Ruff et al., 1988; Fleidervish et al., 1996). In skeletal muscle, slow inactivation has been suggested to regulate the availability of resting sodium channels and to underlie differences in fast- and slow-twitch muscles (Ruff et al., 1987). In neuronal preparations, Fleidervish et al. (1996) suggested its role in spike frequency adaptation and termination of action potential bursts. However, whether slow inactivation actually occurs in vivo has been questioned because of its usual induction by long, sustained depolarizations, which may rarely occur under normal physiological conditions in the brain. Typically, the time scale of onset as well as recovery is regarded to be several seconds (Toib et al., 1998; Ruff et al., 1988; Featherstone et al., 1996). However, some other studies predicted a faster onset of slow inactivation relative to its recovery, because a shorter prepulse (19–350 ms) could induce slow inactivation (Quandt, 1988; Rudy, 1981). The question of whether slow inactivation can be induced by physiologically realistic stimuli such as a very short depolarization or a train of depolarizations is critical to revealing the physiological role of slow inactivation but has remained unanswered for neurons.

A form of inactivation, described by us and others (Jung et al., 1997; Colbert et al., 1997; Martina and Jonas, 1997), was found to be induced by a train of depolarizations and has an accumulative property. We called this "prolonged inactivation" for two reasons. First, its onset appeared to be fast compared to its recovery. Second, it was an open question whether this form of inactivation is basically the same as slow inactivation, considering that no studies of slow inactivation had been performed in CA1 pyramidal cells. Two experimental findings in this study indicate, however, that prolonged inactivation is functionally indistinguishable from slow inactivation. First, both brief and long pulses induce a slowly recovering form of inactivation with a very similar recovery time constant (compare Figs. 6 and 8). This result suggests that short or long depolarizations lead dendritic sodium channels into the same inactivation state, which is slow to recover. Second, prolonged inactivation is prevented by a preceding long depolarization, which drives channels into the slow inactivation state. Because even a 50-Hz train does not exhibit prolonged inactivation after a sustained depolarization (Fig. 9), it appears that sustained depolarization may drive sodium channels into the same inactivation state as a train of depolarizations.

Furthermore, we were able to simulate most aspects of our experimental data by using a model with a single slow inactivation state. Therefore, we feel it is most appropriate to adopt the more common term "slow inactivation" in favor of "prolonged inactivation." This term is appropriate for both historical and logical reasons. First, several properties

data (model 1 recovery τ = 805 ms; model 2 recovery τ = 800 ms). (*Insets*) The first currents from the train at an increased time scale, to demonstrate the kinetics of the current. The dashed lines show the fit of three dendritic patches with the slowest inactivation during a 20-Hz train. The left sidebar refers to train simulation for both models, and the right sidebar refers to both insets. (*C*) Models 1 and 2 differ in response to a long prepulse. Model 1 (*top left*) continues to slowly inactivate during a train of depolarizing pulses, whereas model 2 (*top right*) qualitatively demonstrates the same lack of further slow inactivation seen in Fig. 9 *A*. The middle panels in *C* plot the fraction of channels in I_{fast} (*gray*) and I_{slow} (*black*) for models 1 and 2 during the prepulse experiment. Note that although both models show fairly rapid increases of entry into I_{slow} during the long prepulse, model 2 enters into I_{slow} more completely. The bottom panels of *C* show an expansion of the first 25 ms of the simulation, plotting the fraction of channels in both I_{fast} and I_{slow}. Model 1 (*bottom left*) has a rapid entry into both states, with the I_{fast} state clearly dominating. Model 2 (*bottom right*) initially has a rapid increase in I_{fast} and a smaller increase in I_{slow}, but the curves eventually cross over (see *middle panel* of *C*), signifying the increased tendency of this model to leave the I_{fast} state for the I_{slow} state.

of slow inactivation induced by trains of depolarizations, such as frequency dependence, accumulation with repetitive depolarization, and enhancement of recovery by a hyperpolarized holding potential, are similar to the properties of slow inactivation originally described for *Myxicola* (Rudy, 1981). Second, the slow component of the onset of inactivation induced by single prepulses in our study was fit well by a single exponential with a time constant of 390 ms (Fig. 7); this is indeed slower, compared to the onset of fast inactivation, by more than two orders of magnitude (τ_{onset} = 0.8 ms; Martina and Jonas, 1997).

Although our model uses a single slow inactivation state, channels can enter I_{slow} via multiple routes. One of these routes is actually quite fast (O to I_{slow}; τ_{onset} = 0.52 ms), and the second route is much slower (I_{fast} to I_{slow}; τ_{onset} = 460 ms). Therefore, sodium channels may enter a single slow inactivation state at nearly 1000-fold different rates under different conditions. During prolonged depolarizations, entry will be slow (mostly I_{fast} to I_{slow}); during trains of action potentials, entry will be much more rapid (O to I_{slow}). Without this fast, direct route (O to I_{slow}) the physiological relevance of slow inactivation would be limited during repetitive action potential firing.

Although we could model most of our findings with a single slow inactivation state, it remains possible that there are, in fact, multiple slow inactivation states. Indeed, some of the experimental data could not be simulated by our simple model. Recovery from slow inactivation appears to have different time courses, depending on the frequency and size of stimuli (see Figs. 3–5), suggesting that there could be more than one slow inactivated state, each having different recovery rates. Our model does not show frequency-dependent recovery, such as from Fig. 3 *C*, nor does it accurately predict the effect that increasing command potentials act to increase the recovery rate, such as shown in Fig. 5 *C*. Although the model does qualitatively exhibt voltage-dependent recovery (like Fig. 4 *C*), the currents at the more extreme deviations from the resting potential have very inaccurate kinetics. To reconcile the model with these empirical data, at least two slow inactivated states should be included in the model: one slow inactivated state, which has a faster recovery, promoted by high-frequency trains or larger command potentials (and possibly hyperpolarizing holding potentials), and at least one other slow inactivated state, with a slower recovery rate, promoted preferentially by either long or short single pulses, slower pulse frequencies, or small voltage steps. The possibility of multiple slow inactivation states is also compatible with some studies of slow inactivation, which demonstrate inactivation on a much longer time scale than the inactivation studied here (Toib et al., 1998; Featherstone et al., 1996; Ruff et al., 1988). It may seem simple to address this question by constructing a model with multiple slow inactivation states. However, such a gating scheme would add another layer of complexity to the model, because then we must determine the states from which the various slow inactivated states are accessible, and at which voltage-dependent rates. In addition, considering the basic assumptions of our model, such as interpreting macroscopic currents with a single-channel model and the homogeneity of channels (see below), it would be prudent to obtain single-channel data before constructing a more elaborate model.

Dendritic versus somatic slow, cumulative inactivation

The degree of slow inactivation has been shown to be different for sodium channels in the dendrites and somata of CA1 pyramidal cells (Colbert et al., 1997; Jung et al., 1997). There are two possible explanations for this finding, which are not mutually exclusive. One possibility is the existence of different types of sodium channels. Although there is immunocytochemical evidence for possible differential distribution of sodium channel α-subunit types between dendritic and somatic regions (Westenbroek et al., 1989), electrophysiological studies in pyramidal cells have not shown any difference between dendritic and somatic sodium channels at the single-channel level (Magee and Johnston, 1995). Therefore, further studies are required to determine the possible contribution of different subunit types of sodium channels for this regional difference. A second possibility is differential modulation of a single type of sodium channel. Modulation of sodium channel behavior through the protein kinase C and protein kinase A pathways or by G proteins has been demonstrated in *Xenopus* oocytes, CHO cell lines, and intact neurons (Li et al., 1992, 1993; Ma et al., 1994). Recently, Colbert et al. (1998) demonstrated that in dendrites, but not somata, activation of PKC decreased the attenuation of sodium currents during a train of depolarizations. The corresponding activity-dependent attenuation of back-propagating action potential amplitude decreased as well. A similar effect of muscarinic receptor activation on back-propagating spikes was shown by Tsubokawa and Ross (1997), suggesting the possibility that differential activation of cholinergic inputs between dendritic and somatic regions may differentially modulate sodium channels in each region.

Together with these data, the finding that the degree of slow inactivation gradually increases with distance from the soma suggests the following scenario. There are likely to be two populations of channels (for one or more reasons discussed above), one that undergoes slow inactivation and another that does not. The proportion of inactivating channels would then determine the degree of slow inactivation at a specific location along dendrites. For this reason, we chose to model the most extreme cases of slow inactivation recorded from dendritic patches stimulated at 20 Hz (indicated by the *dashed lines* in Fig. 10), because these are likely to represent the most homogeneous population of channels. Despite the inhomogeneity of channels along the somatodendritic axis, the time course of recovery from slow inactivation is independent of the distance from the soma, as the recovery time course will only be determined by the

population of channels that undergoes slow inactivation. The gradual rather than abrupt change in the degree of slow inactivation along the somatodendritic axis could be explained by postulating that the fraction of noninactivating channels decreases gradually along the distance from the soma. Biochemically, there could be a number of mechanisms to explain this gradual change. For example, factors may exist that could limit the insertion of certain types of channel subunits in the dendrites. Alternatively, decreases in diffusible proteins along the dendrites that modulate the channels posttranslationally may be another possible mechanism.

Physiological implications of slow inactivation

Although the experiments reported here have attempted to mimic conditions that are as physiological as possible, the situation is much more complicated for real neurons. In particular, various locations throughout the dendrites will experience back-propagating action potentials of different amplitudes. This is especially true during repetitive firing of the neuron, as the amplitude of the back-propagating action potentials decreases during the train because of slow inactivation itself. Some of the later spikes in a train may even be propagating completely passively, so that sodium channels are not even activated (Spruston et al., 1995). Therefore it is important to understand how the properties of slow inactivation will affect the way back-propagating action potentials invade dendrites.

One factor that will affect back-propagating action potentials is the frequency dependence of slow inactivation. High-frequency trains of back-propagating action potentials are less effective in invading the dendritic tree than low-frequency trains or single action potentials. This can be explained in part because higher frequency trains will induce more slow inactivation of sodium channels (Fig. 3 *A*). Because this frequency effect increases in the dendrites, it will tend to increase the amount of attenuation of back-propagating action potentials. However, higher frequency trains also act to accelerate the recovery of channels from slow inactivation (Fig. 3 *B*). Therefore, higher frequency trains influence the availability of sodium channels in two opposing ways by increasing both the induction and the recovery of slow inactivation.

The size of previous back-propagating action potentials will also affect slow inactivation along the dendrites, although in a complicated manner. A single back-propagating action potential will tend to make distal dendrites less available for further excitation than proximal dendrites, because the action potential will inactivate sodium channels along its path. This same action potential will also be able to promote more recovery in the proximal dendrites, because the amplitude of the spike will be greater (Fig. 5). During trains of action potentials, early action potentials in the train will induce slow inactivation, whereas later spikes, especially during high-frequency stimulation, will provide less depolarization in distal dendrites, thus allowing the recovery of distal sodium channels from slow inactivation, even during continuous action potential firing.

The local membrane potential will also affect how action potentials back-propagate. The results presented here (Fig. 4) and previously suggest that hyperpolarizations act to accelerate recovery from slow inactivation (Jung et al., 1997; Colbert et al., 1997), which is consistent with a similar hyperpolarization-induced increase in recovery of back-propagating action potential amplitude after a train of spikes (Spruston et al., 1995). However, the nature of this hyperpolarization must be carefully considered, because appropriately timed inhibitory postsynaptic potentials have been shown to decrease the amplitude of back-propagating action potentials (Tsubokawa and Ross, 1996). This reduction is most likely due to a shunting of the membrane conductance, perhaps through activation of $GABA_A$ receptors. It is also interesting to note that holding the dendrites at 20 mV depolarized relative to rest does not affect slow inactivation and its recovery. This is compatible with the result shown by Spruston et al. (1995), in which subthreshold depolarizing current injections do not reduce the amplitude of subsequent back-propagating action potentials.

Recently, both in vivo and in vitro studies have demonstrated that dendrites of CA1 pyramidal cells can generate dendritic spikes, which sometimes do not propagate to the soma (Golding and Spruston, 1998; Kamondi et al., 1998a). Sodium channel availability can therefore be changed by any slow inactivation induced by these local dendritic spikes. The properties of slow inactivation associated with dendritic spikes affect the further excitability of dendrites in more or less the same manner as back-propagating action potentials do. However, as dendritic spike amplitude at any specific dendritic location is much more variable than the amplitude of a single back-propagating action potential, the effects of spike amplitude on sodium channel recovery could be very different (Golding and Spruston, 1998; Kamondi et al., 1998a). Therefore, as the size of dendritic spikes changes, the further availability of sodium channels can also be modulated in that particular dendritic location. Another difference between dendritic spikes and back-propagating action potentials is that dendritic spikes can be more spatially restricted. Thus any effects of dendritic spikes on slow inactivation could be more localized than the effects of back-propagating action potentials. For example, a dendritic spike localized to a single dendritic branch might limit subsequent action potential back-propagation into that branch, but not others.

In vivo, interactions of back-propagating action potentials and dendritic spikes will lead to highly variable amounts of slow inactivation of sodium channels throughout a neuron that can affect synaptic integration by influencing the further back-propagation or generation of dendritic spikes in various regions of the dendrites. Taken together with the possible metabolic modulation of slow inactivation (Colbert and Johnston, 1998) and the role of back-propagating action potentials on long-term potentia-

tion (Magee and Johnston, 1997), our results suggest that slow inactivation will play an important role in the integration of synaptic events and possibly synaptic plasticity.

Slow inactivation of sodium channels creates an intricate background of modulation of neuronal excitability against which synaptic integration and action potential initiation will occur. To completely understand and predict how neurons will behave, especially in the context of networks of interconnected cells, accurate models must be created. These models must precisely represent neuronal morphology and passive properties, which underlie the basic properties of synaptic integration, as well as the detailed biophysics of sodium channels and other channels creating active responses to synaptic stimuli.

We thank Drs. David Colquhoun, Nace Golding, Indira Raman, and Jay Yeh for their discussion and comments on the manuscript, and Arnd Roth for help with the modeling.

NS was supported by the National Institute of Neurological Disorders and Stroke (grant N35180), the Human Frontiers in Science Program, and a Sloan Fellowship. TM was supported by training grant T32GM08061 from the National Institutes of Health.

REFERENCES

Callaway, J. C., and W. N. Ross. 1995. Frequency-dependent propagation of sodium action potentials in dendrites of hippocampal CA1 pyramidal neurons. *J. Neurophysiol.* 74:1395–1403.

Colbert, C. M., and D. Johnston. 1998. Protein kinase C activation decreases activity-dependent attenuation of dendritic Na^+ current in hippocampal CA1 pyramidal neurons. *J. Neurophysiol.* 79:491–495.

Colbert, C. M., J. C. Magee, D. A. Hoffman, and D. Johnston. 1997. Slow recovery from inactivation of Na^+ channels underlies the activity-dependent attenuation of dendritic action potentials in hippocampal CA1 pyramidal neurons. *J. Neurosci.* 17:6512–6521.

Colquhoun, D., and A. G. Hawkes. 1982. On the stochastic properties of bursts of single ion channel openings and of clusters of bursts. *Phil. Trans. R. Soc. Lond. (Biol.)* 300:1–59.

Debanne, D., B. H. Gahwiler, and S. M. Thompson. 1998. Long-term synaptic plasticity between pairs of individual CA3 pyramidal cells in rat hippocampal slice cultures. *J. Physiol. (Lond.).* 507:237–247.

Featherstone, D. E., J. E. Richmond, and P. C. Ruben. 1996. Interaction between fast and slow inactivation in Skm1 sodium channels. *Biophys. J.* 71:3098–3109.

Fleidervish, I. A., A. Friedman, and M. J. Gutnick. 1996. Slow inactivation of Na^+ current and slow cumulative spike adaptation in mouse and guinea-pig neocortical neurones in slices. *J. Physiol. (Lond.).* 493: 83–97.

Golding, N. L., and N. Spruston. 1998. Dendritic sodium spikes are variable triggers of axonal action potentials in hippocampal CA1 pyramidal neurons. *Neuron.* 21:1189–1200.

Jung, H. Y., T. Mickus, and N. Spruston. 1997. Prolonged sodium channel inactivation contributes to dendritic action potential attenuation in hippocampal pyramidal neurons. *J. Neurosci.* 17:6639–6646.

Kamondi, A., L. Acsady, and G. Buzsaki. 1998a. Dendritic spikes are enhanced by cooperative network activity in the intact hippocampus. *J Neurosci.* 18:3919–3928.

Kamondi, A., L. Acsady, X.-J. Wang, and G. Buzsaki. 1998b. Theta oscillations in somata and dendrites of hippocampal pyramidal cells in vivo: activity-dependent phase-precession of action potentials. *Hippocampus.* 8:244–261.

Li, M., J. West, Y. Lai, T. Scheuer, and W. Catterall. 1992. Functional modulation of brain sodium channels by cAMP-dependent phosphorylation. *Neuron.* 8:1151–1159.

Li, M., J. West, R. Numann, B. Murphy, T. Scheuer, and W. Catterall. 1993. Convergent regulation of sodium channels by protein kinase C and cAMP-dependent protein kinase. *Science.* 261:1439–1442.

Ma, J., M. Li, W. Catterall, and T. Scheuer. 1994. Modulation of brain Na^+ channels by a G protein coupled pathway. *Proc. Natl. Acad. Sci. USA.* 91:12351–12355.

Magee, J., and D. Johnston. 1995. Characterization of single voltage-gated Na^+ and Ca^{2+} channels in apical dendrites of rat CA1 pyramidal neurons. *J. Physiol. (Lond.).* 487:67–90.

Magee, J., and D. Johnston. 1997. A synaptically controlled, associative signal for Hebbian plasticity in hippocampal neurons. *Science.* 275: 209–212.

Markram, H., J. Lubke, M. Frotscher, and B. Sakmann. 1997. Regulation of synaptic efficacy by coincidence of postsynpatic APs and EPSPs. *Science.* 275:213–215.

Martina, M., and P. Jonas. 1997. Functional differences in Na^+ channel gating between fast-spiking interneurones and principal neurones of rat hippocampus. *J. Physiol. (Lond.).* 505:593–603.

Migliore, M. 1996. Modeling the attenuation and failure of action potentials in the dendrites of hippocampal neurons. *Biophys. J.* 71: 2394–2403.

Narahashi, T. 1964. Restoration of action potential by anodal polarization in lobster giant axon. *J. Cell. Comp. Physiol.* 64:73–96.

Patlak, J. 1991. Molecular kinetics of voltage-dependent Na^+ channels. *Physiol. Rev.* 71:1047–1080.

Quandt, F. N. 1988. Modification of slow inactivation of single sodium channels by phenytoin in neuroblastoma cells. *Mol. Pharmacol.* 34: 557–565.

Rudy, B. 1978. Slow inactivation of the sodium conductance in squid giant axons. Pronase resistance. *J. Physiol. (Lond.).* 283:1–21.

Rudy, B. 1981. Inactivation in *Myxicola* giant axons responsible for slow and accumulative adaptation phenomena. *J. Physiol. (Lond.).* 312: 531–549.

Ruff, R. L. 1996. Single-channel basis of slow inactivation of Na^+ channels in rat skeletal muscle. *Am. J. Physiol.* 271:C971–C981.

Ruff, R. L., L. Simoncini, and W. Stuhmer. 1987. Comparison between slow sodium channel inactivation in rat slow- and fast-twitch muscle. *J. Physiol. (Lond.).* 383:339–348.

Ruff, R. L., L. Simoncini, and W. Stuhmer. 1988. Slow sodium channel inactivation in mammalian muscle: a possible role in regulating excitability. *Muscle Nerve.* 11:502–510.

Soltesz, I., and M. Deschenes. 1993. Low- and high-frequency membrane potential oscillations during theta activity in CA1 and CA3 pyramidal neurons of the rat hippocampus under ketamine-xylazine anesthesia. *J. Neurophysiol.* 70:97–116.

Spruston, N., Y. Schiller, G. Stuart, and B. Sakmann. 1995. Activity-dependent action potential invasion and calcium influx into hippocampal CA1 dendrites. *Science.* 268:297–300.

Starkus, J. G., and P. Shrager. 1978. Modification of slow sodium inactivation in nerve after internal perfusion with trypsin. *Am. J. Physiol.* 235:C238–C244.

Stuart, G., H.-U. Dodt, and B. Sakmann. 1993. Patch-clamp recordings from the soma and dendrites of neurons in brain slices using infrared video microscopy. *Pflügers Arch.* 423:511–518.

Stuart, G., N. Spruston, B. Sakmann, and M. Häusser. 1997. Action potential initiation and backpropagation in neurons of the mammalian CNS. *Trends Neurosci.* 20:125–131.

Toib, A., V. Lyakhov, and S. Marom. 1998. Interaction between duration of activity and time course of recovery from slow inactivation in mammalian brain Na^+ channels. *J. Neurosci.* 18:1893–1903.

Tsubokawa, H., and W. N. Ross. 1996. IPSPs modulate spike backpropagation and associated $[Ca^{2+}]_i$ changes in the dendrites of hippocampal CA1 pyramidal neurons. *J. Neurophysiol.* 76:2896–2906.

Tsubokawa, H., and W. N. Ross. 1997. Muscarinic modulation of spike backpropagation in the apical dendrites of hippocampal CA1 pyramidal neurons. *J. Neurosci.* 17:5782–5791.

Westenbroek, R., D. Merrick, and W. Catterall. 1989. Differential subcellular localization of the RI and RII Na^+ channel subtypes in central neurons. *Neuron.* 3:695–704.